A Regional-Scale Evaluation of Changes in Environmental Stability for Summertime Afternoon Precipitation under Global Warming from Super-High-Resolution GCM Simulations: A Study for the Case in the Kanto Plain

Tetsuya TAKEMI, Syohei NOMURA[1], Yuichiro OKU[2], and Hirohiko ISHIKAWA

Disaster Prevention Research Institute, Kyoto University, Uji, Japan

(*Manuscript received 8 March 2011, in final form 22 September 2011*)

Abstract

Understanding and forecasting of summertime afternoon precipitation due to rapidly developing cumulonimbus clouds without any significant synoptic-scale influences are important to prevent and mitigate the induced disasters. Future changes in the behavior of such precipitation events have recently gained scientific and societal interests. This study investigates the environmental stability for afternoon precipitation that develops under synoptically undisturbed conditions in summer by using the outputs of 20-km-mesh, super-high-resolution atmospheric general circulation model (GCM) simulations for a present, a near-future, and a future climate under global warming with the Intergovernmental Panel on Climate Change A1B emission scenario. The Kanto Plain was chosen as the analysis area. After verifying the usefulness of the GCM present-climate outputs with observations and gridded mesoscale analyses, we examine the future changes in the environmental stability for the afternoon precipitation by conducting statistical analyses. In the future climates, temperature lapse rate decreased in the lower troposphere, while water vapor mixing ratio increased throughout the deep troposphere. The changes in the temperature and moisture profiles resulted in the increase in both precipitable water vapor and convective available potential energy. These projected changes will be enhanced with the future period. Furthermore, the statistical analyses for the differences of the stability parameters between no-rain and rain days under the synoptically undisturbed condition in each simulated climate period indicated that the representations of the stability parameters that distinguish no-rain and rain events are basically unchanged between the present and the future climates. This result suggests that the environmental characteristics favorable for afternoon precipitation in the synoptically undisturbed environments will not change under global warming.

1. Introduction

Severe local rainfalls have potentially high societal impacts in many regions of the world. Significant efforts from both research and operational sector have been made on the understanding and forecasting those events from planetary-scale, synoptic-scale, and mesoscale perspectives. Rapid developments in observational and computational resources have nowadays enabled us to focus more on convective-scales that are on the order of 1 km. Specifically, local-scale convective rainfalls due to rapidly developing cumulonimbus clouds without any significant synoptic influences have been one of the main research issues. It is anticipated that such rapidly developing, convective rainfalls under synoptically undisturbed conditions would become more prevalent and more intensified in a future warming climate. In the Fourth Assessment Report (AR4) by the Intergovermental Panel on Climate

Corresponding author: Tetsuya Takemi, Disaster Prevention Research Institute, Kyoto University, Goka-sho, Uji, Kyoto 611-0011, Japan.
E-mail: takemi.tetsuya.8r@kyoto-u.ac.jp
1 Present affiliation: Narita International Airport Corporation.
2 Present affiliation: Osaka City Institute of Public Health and Environmental Sciences.

Change (IPCC) (2007), it is stated that the intensity of precipitation events is projected to increase particularly in tropical and high latitude areas, and that precipitation extremes are more enhanced than the precipitation means in most tropical and mid- and high-latitude areas.

Future projections of precipitation characteristics not only in global-scales but also in regional-scales were investigated through numerical simulations with the use of general circulation models (GCMs) and regional climate models (RCMs) nested in GCMs. For cases in Japan, as an example, the general characteristics of the changes in precipitation over Japan were investigated by GCM studies (e.g., Kimoto et al. 2005; Kamiguchi et al. 2006), and the changes in precipitation behavior due specifically to Baiu frontal activities were also focused on, owing to the significance and frequency of heavy rainfalls during the Baiu periods in Japan, by many studies with both GCMs (Kusunoki et al. 2006; Kitoh and Uchiyama 2006; Ninomiya 2009) and RCMs (Yoshizaki et al. 2005; Kanada et al. 2005; Wakazuki et al. 2005; Yasunaga et al. 2006). Although the quantitative analyses on the characteristics of Baiu precipitation under global warming were extensively investigated, there have been few studies that investigated the convective precipitation in synoptically undisturbed environments under global warming, owing to fine-scales of such convective precipitation for numerical representations.

The future projections will benefit much from the observational evidences revealed by the past records. The long-term variability of the general characteristics of precipitation for cases in Japan has been investigated from statistical viewpoints by many studies such as Yonetani (1982), Iwashima and Yamamoto (1993), Fujibe (1998), Sato and Takahashi (2000), Kanae et al. (2004), Fujibe et al. (2005, 2006, 2009), Kamiguchi et al. (2010), and Iwasaki (2010). There have been arguments on the reason for the changes in the frequency and intensity of precipitation: some studies attributed to global climate change (i.e., warming); and others implied the effects of urbanization. However, the stability conditions of the environmental atmosphere should also play a critical role in controlling the behavior of convective rainfalls.

There are studies that emphasized the importance of environmental conditions for convective storms and precipitation. For the change in tropical cyclone climatology due to global warming, Sugi et al. (2002) considered that the decrease in the number of tropical cyclones is due to more stabilized atmosphere and hence more weakened tropical circulation. From the modeling studies it is well known that the tropical troposphere will be more stabilized in a warming climate; this modeled trend has been shown to be consistent with the observations (Santer et al. 2005, 2008; Thorne et al. 2010), but with some exaggeration in the GCM simulations (Fu et al. 2011). On the other hand, some studies indicated from the observations and reanalysis data that the increase in the free tropospheric temperature in the Tropics is smaller than the temperature increase at the surface (Christy et al. 2007; Bengston and Hodges 2011), which means that the stability of the tropical troposphere decreases in a warming climate. In addition, the differences in the temperature trends in the lower and upper troposphere widely vary over the globe (Bengston and Hodges 2011) and in the latitude (Thorne et al. 2010). Therefore, it is not obvious whether the tropospheric stability increases also in extra-tropical regions in any seasons and any meteorological settings. Considering this uncertainty, the changes in environmental stability conditions for the convective rainfalls in the undisturbed settings need to be investigated from a regional-scale point of view.

For the case in Japan in summer, Kanada et al. (2010a) examined the daily precipitation and the atmospheric state in July (which corresponds to the Baiu period) by conducting the RCM simulations and found that static stability, moisture content, and convective available potential energy (CAPE) are more increased in the future climates than in the present. They further noted that the increased CAPE would lead to stronger updrafts and therefore more intense precipitation. Del Genio et al. (2007) also pointed out that due to increased CAPE updrafts become stronger in global warming climate in their investigations for continental deep convection within a GCM simulation. From cloud-resolving simulations in idealized settings that represent horizontally homogeneous, undisturbed conditions, Takemi (2007, 2010) investigated the effects of static stability on the intensities of convection and precipitation and suggested that stability diagnosis for the climate simulation data should be useful for examining the variation of precipitation characteristics in the simulated climate.

Nomura and Takemi (2011, hereafter NT11) have recently investigated the environmental stability for summertime afternoon precipitation under

synoptically undisturbed environments over the Kanto Plain, a region that includes the Tokyo metropolitan area in Japan, in terms of commonly used stability indices and parameters. They used the gridded mesoscale analysis data at the regional-scale after validating the data against radiosonde observations. Their analyses on the differences of temperature and humidity at each height between no-rain and rainy cases indicated that the temperatures and moistures at low to middle levels clearly distinguish the stability conditions for the afternoon rain events, which confirmed previous observational studies by Yonetani (1975), Taguchi et al. (2002), and Kawano et al. (2004) who examined the environmental conditions by using radiosonde data at a single site in the northern part of the Kanto Plain. The idea of these studies can be applied to climate-simulation data to investigate the long-term trend of the changes in the environmental conditions for convective precipitation.

In this study, we investigate the environmental stability for convective rain events in synoptically undisturbed conditions from climate-simulation data and evaluate the changes in the environmental stability at a regional-scale under global warming. According to Chuda and Niino (2005), stability conditions widely change over Japan depending on locations and seasons; therefore, we focus on the summertime cases in the Kanto Plain where a number of studies have been previously done for environmental conditions. Moreover, the study of Chuda and Niino strongly suggests that the environmental conditions that control the development of cumulus convection will not be unchanged if the climate is changed from a region to a region, from a season to a season, and furthermore from the present to the future. Thus, the evaluation of convective potential for the future periods is of scientific interest. Since the focus of this study is to evaluate the environmental conditions, high-resolution GCM data are considered to sufficiently resolve and represent the environments and therefore to be useful. The outputs of super-high-resolution global climate simulations with a warming-climate scenario are used to examine stability parameters for rain events over the Kanto Plain. Although it is well known from GCM simulations that the stability increases in the tropical atmosphere under global warming, the environmental changes in extra-tropical regions in undisturbed meteorological conditions have not been explicitly investigated. The purpose of this study is to provide a regional-scale evaluation of the environmental changes for convective precipitation under synoptically undisturbed conditions in a warming climate.

2. GCM data and analysis procedure

2.1 GCM and data

The data used in this study are the gridded outputs at a 20-km horizontal spacing of the super-high-resolution atmospheric GCM (AGCM) simulations at a resolution of T959L60 (i.e., triangular truncation of 959 with 60 vertical layers) for present, near-future, and century-end future climates, conducted by Meteorological Research Institute (MRI), Japan Meteorological Agency (JMA) under the Innovative Program of Climate Change Projection for the 21st Century (the KAKUSHIN program). The code name of this AGCM is MRI-AGCM3.2S. The outline of the relevant KAKUSHIN program and the details of the AGCM were given by Kitoh et al. (2009) and Murakami and Wang (2010). This super-high-resolution AGCM was originally developed by Mizuta et al. (2006), and the present-climate simulations were well validated against observations in their study. This AGCM was extensively used for the future projections of the Baiu rainfalls (Kusunoki et al. 2006), typhoons (Murakami et al. 2011), and other climate applications.

The GCM simulations are intended to represent the present climate (during 1979–2008), the near-future climate (during 2015–2044), and the last quarter of the twenty-first century (during 2074–2104), each for 30 years with a global warming scenario, that is, the IPCC A1B emission scenario (IPCC 2007). The preliminary experiments were intended for 25-year periods (1979–2003, 2015–2039, and 2075–2099), and Kitoh et al. (2009) confirmed that the preliminary results were almost the same as those in Mizuta et al. (2006). Therefore, it is expected that the GCM results used in this study have good performance in representing the present climate. In this study, we used the outputs simulated for 25-year periods that correspond to 1980–2004 for the present climate, 2020–2044 for the near-future climate, and 2075–2099 for the century-end future climate. Hereafter, these periods are referred to simply as the present, the near-future, and the future, respectively.

The present focus is on the regional-scale atmospheric states that are the environments for summertime afternoon precipitation events under synoptically undisturbed conditions. In order to
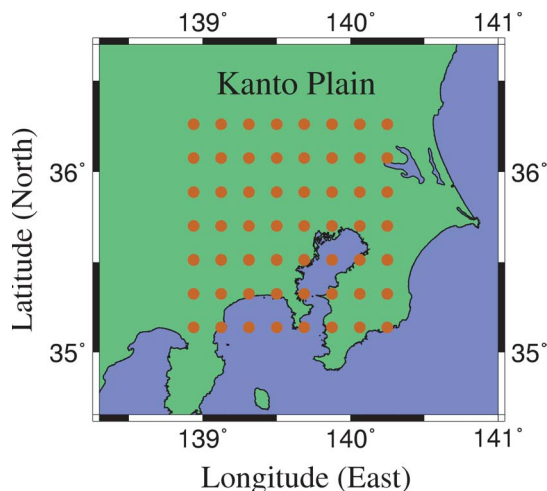
Fig. 1. The map of the Kanto Plain and the surroundings and the locations of the GCM grid points (red points) representing the analysis area of the present study.

examine the performance of the GCM present-climate simulation in representing the existing real climate for the undisturbed environments intended in this study, we use the upper-air radiosonde observations at the Tateno site in Tsukuba, Ibaraki and the numerical analysis data from the JMA's operational Mesoscale Model (MSM). The periods of these data used are the same as in NT11: during 1976–2010 for the radiosonde data; and during 2002–2010 for the MSM data. We also use precipitation data which are obtained from the Automated Meteorological Data Acquisition System (AMeDAS) observations.

The analysis area is a mesoscale region of about 100 km by 100 km centered at around central Tokyo (i.e., 35.14°N–36.26°N and 138.94°E–142.25°E), which covers the most part of the Kanto Plain. This area is almost the same as examined in NT11. Figure 1 shows the area of interest and the data points of the gridded GCM outputs. The time intervals of surface and upper-air variables from the GCM outputs are 1 hour and 6 hours, respectively. As described shortly in the next subsection, the data of August are used to better focus on synoptically undisturbed conditions in summer.

2.2 Analysis procedure

In NT11, synoptically undisturbed conditions in summer were chosen with the following procedure. At first, days with daily maximum temperature of 30°C or greater at any AMeDAS sites in the analysis area were chosen. The second step was to choose days when precipitation in the morning hours was not observed at all the AMeDAS sites in the analysis area. The third step was to exclude days that were considered to be affected by fronts and typhoons by examining weather charts, typhoon best-track data, and Baiu-period definitions of JMA. The last step was to choose days when the MSM predicted successfully afternoon rain/no-rain events. All these steps assumed the use of the observation data. However, weather charts and Baiu-period definitions are not available in the future-climate simulations. Therefore, an objective approach is desired in order to extract days with no significant synoptic-scale forcings from the GCM simulation outputs.

For the purpose of setting an objective approach, the vertical profiles of wind speeds are examined from radiosonde observations. Figure 2 indicates the composited profiles of wind speeds for no-rain (referred to as N in NT11), rain (referred to as R in NT11), and strong rain cases (referred to as S in NT11) from the 35-year radiosonde data at Tateno at 0900 JST[1]. Wind shears and upper-level wind speeds are generally quite small, compared with typical continental environments for severe storms and squall lines (Bluestein and Jain 1985). Based on these wind profiles, an objective approach to extract the summertime undisturbed conditions from the GCM outputs is to set the criteria as follows:

1) Use the data only for August to avoid including the Baiu periods;
2) Exclude days under conditions with 500-hPa wind speed of equal to or greater than 10 m s^{-1} and wind-speed difference between the 500- and 975-hPa levels of equal to or greater than 8 m s^{-1};
3) Choose days having rainfall of less than 1 mm during the morning period (i.e., from 0000 to 1200 JST) at all the grids in the analysis area.

Hereafter we refer to the states that pass these three criteria as synoptically undisturbed condition. To apply these criteria, the GCM data are averaged over the analysis area at each vertical level, and then the shear and velocity are calculated from the area-averaged values.

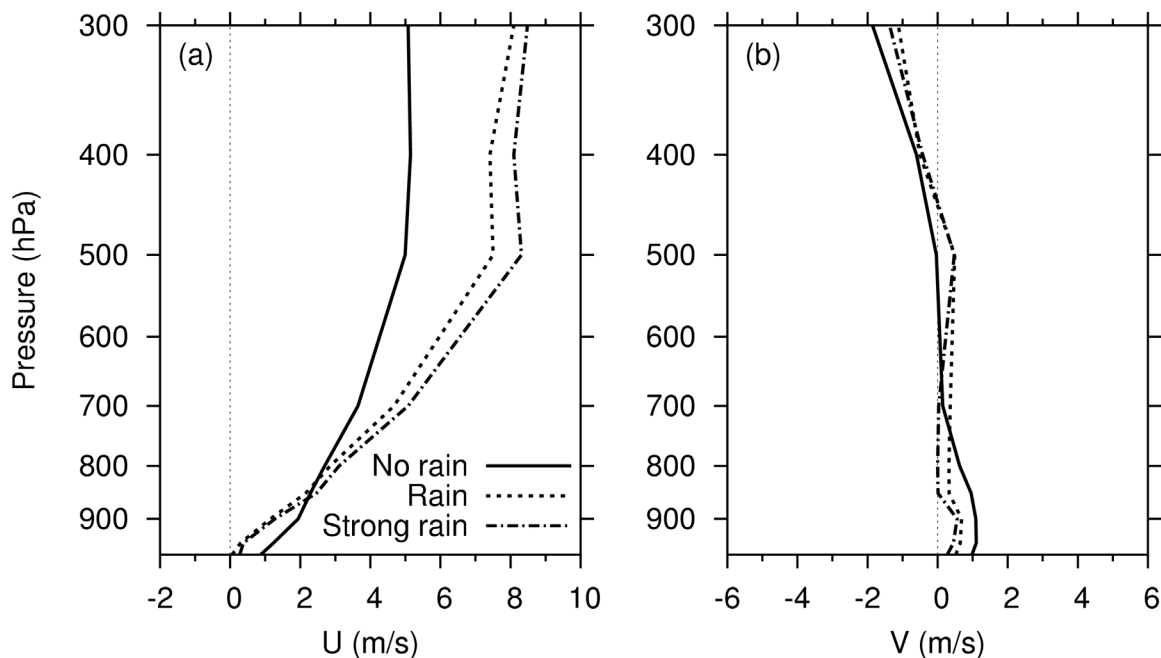1   Japan Standard Time, which is 9 hours plus UTC.

Fig. 2.   The vertical profiles of (a) the east-west and (b) the north-south components of wind speed averaged
for each rain category under the synoptically undisturbed condition from the 35-year radiosonde data at
the Tateno site. The solid lines denote the no-rain case, the dotted lines the rain case, and the dash-dotted
lines the strong-rain case. See Nomura and Takemi (2011) for the definitions of these cases.

Figure 3 compares the two approaches, that is, the NT11 method and the present objective approach, in terms of the averaged vertical profiles of temperature and relative humidity from the 35-year radiosonde data at 0900 JST under the synoptically undisturbed conditions. The number of days chosen by the NT11 method was 699, while that by the present approach was 344. Although the number of days chosen by the present approach is significantly smaller than that by NT11, 300 cases out of the selected 344 cases satisfy the condition of NT11. The averaged profiles based on the present approach are closely coincident with the averages by the NT11 method. The present approach was also compared with the NT11 method against the 9-year MSM data (not shown); this comparison indicated that 69 cases out of the total 76 cases extracted by the present procedure satisfied the NT11 condition. Note here that the number of the cases chosen in NT11 from the MSM data was 124. Therefore, the present objective approach based on the wind shear and the upper-level wind speed performs reasonably well in choosing the synoptically undisturbed condition.

In the following sections, we describe the charac-teristics of environmental stability under synoptically undisturbed conditions represented in the GCM simulations for the present, the near-future, and the future climates. The stability indices and parameters examined in this study are the same as in NT11; namely, CAPE, convective inhibition (CIN), lifting condensation level (LCL), level of free convection (LFC), level of neutral buoyancy (LNB), Showalter stability index (SSI), lifted index (LI), K-index (KI), total-totals index (TT), precipitable water (PW), and temperature lapse rate from 950 hPa to 500 hPa (TLR). The definitions of these parameters except TLR can be found in standard textbooks such as Bluestein (1993). Temperature lapse rate in the lower half of the troposphere is chosen since it was found that this lapse rate significantly regulates the intensity of convective precipitation under idealized modeling settings (Takemi 2007, 2010). Note that the present study examines the parameters specifically related to the temperature and moisture profiles in weak-shear environments and therefore shear-related parameters such as bulk Richardson number and storm-relative helicity are beyond the scope of the present study.
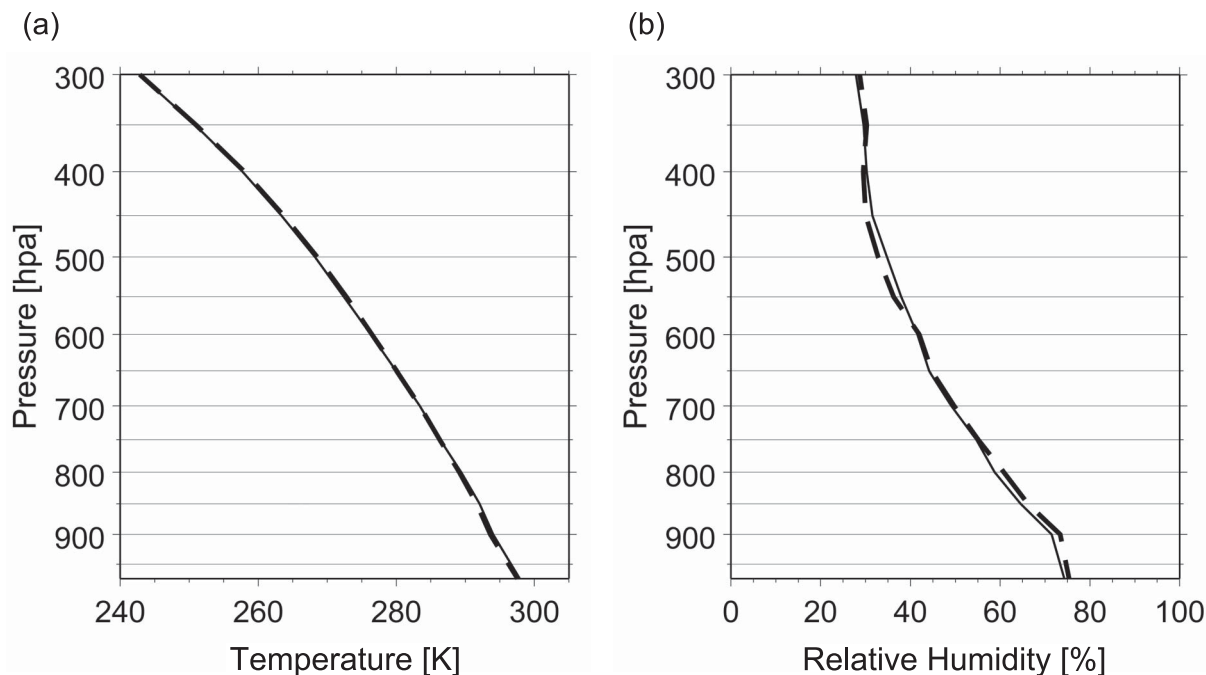
(a)

(b)

Fig. 3. The vertical profiles of (a) temperature and (b) relative humidity at the Tateno site averaged for the synoptically undisturbed conditions which are determined by the method used by Nomura and Takemi (2011) (solid line) and the present objective procedure (dashed line).

3. Results

3.1 Representation of the undisturbed condition in the present-climate simulation

As described in Sections 1 and 2.1, the performance of the present GCM simulations has been well tested and evaluated in terms of seasonal and/or monthly climatologies, and thus the outputs of the present GCM have been used for various applications. To our knowledge, however, there have been little studies that investigated the environmental conditions for convection and precipitation under synoptically undisturbed conditions by using the GCM outputs. Therefore, the representation of the synoptically undisturbed condition in the present-climate simulation is evaluated here.

By applying the criteria described in Section 2.2 against the present-climate simulation, we found that there were 182 days that passed the criteria among the total number (i.e., 775) of days in August during the 25 years. In this subsection, the general characteristics such as temperature and moisture profiles as well as stability parameters for the 182 days are examined and are compared with the data used in NT11.

Figure 4 compares the vertical profiles of temperature, relative humidity, and water vapor mixing ratio averaged for the synoptically undisturbed cases obtained from the GCM present-climate simulation, the 35-year radiosonde observations at Tateno, and the 9-year MSM analyses over the analysis area used in NT11. Note that the GCM data were extracted by the present objective procedure while the radiosonde and MSM data were extracted by the method used in NT11; the idea is to examine how the undisturbed conditions in the real cases are represented in the GCM present-climate simulation. The figure indicates that the temperature and mixing ratio profiles obtained from the GCM outputs seem to in general reproduce the existing climates obtained by the observations and the numerical analyses, although there are some noticeable differences between the GCM climate and the observations/analyses. The temperature profiles indicate that there is a colder bias below about the 800-hPa level in the GCM than in the radiosonde observations, while the mixing ratio profiles show that the amounts at the middle levels in the GCM are smaller than those in the observations. The difference between the GCM results and the radio-
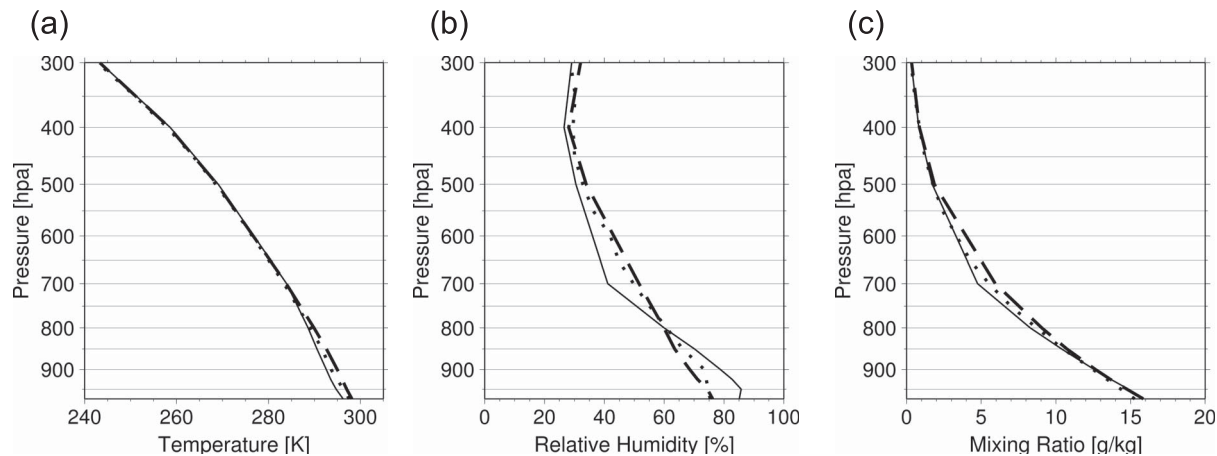
Fig. 4. The vertical profiles of (a) temperature, (b) relative humidity, and (c) water vapor mixing ratio averaged for the synoptically undisturbed condition, obtained from the GCM present simulation (solid lines), the Tateno radiosonde observations (dotted lines), and the MSM analyses (dashed lines).

sonde observations in the profile of relative humidity appears to be more pronounced; this relative humidity difference seems to be closely linked to the low-level colder bias and the middle-level drier bias in the GCM simulations.

Figure 4 also shows that the MSM temperature (mixing ratio) profile has a warmer (moister) bias below (above) the 800-hPa level, which is opposite to the GCM bias. Because the GCM and MSM data both have some biases against the radiosonde observations, it is not appropriate to think that only the GCM simulation fails to accurately represent the observed climate. It is fair to say that both GCM and MSM cannot be free from a certain amount of biases, although the biases seen in the GCM data are somewhat larger than those in the MSM analyses.

The comparison between the GCM data and the observations/analyses is further extended to the stability parameters examined in this study. The frequency distributions of the stability parameters for the undisturbed conditions among the GCM data, the observations, and the MSM analyses are compared in Fig. 5. Among the parameters, the distributions for SSI, LI, CAPE, LCL, and LNB obtained by the GCM outputs agree quite well with those obtained by the radiosonde observations as well as the MSM analyses. The distributions for most of the other parameters obtained from the observations/analyses are also represented favorably in the GCM data, although the differences between the GCM data and the observations are seen

to be large in the distributions of TLR and CIN. These differences in TLR and CIN are considered to be due to the representation of the temperature profile in the lowest layer in GCM (Fig. 4a). There is a colder bias below the 800-hPa level in GCM, which leads to the decrease in the magnitude of TLR. On the other hand, the lapse rate below about the 900-hPa level in GCM is close to the dry adiabat, which tends to reduce the magnitude of CIN.

From the comparisons indicated in Figs. 4 and 5 it is said that the present climate in the GCM data captures the overall features obtained from the observations and analyses considerably well. There are of course noticeable differences between the GCM data and the observations/analyses. Among the differences, the bias of the temperature profile in GCM from the observations is more pronounced (Figs. 4a, 5f) and may not be negligible. In the followings, we are mostly interested in the anomalies of the environmental conditions in the future and near-future climate from those in the present climate. It may be safely to assume that, as a first approximation, the biases of the GCM simulations will appear in the future climates in the same way as in the present climate. Therefore, the biases such as in TLR and CIN will not be significant in discussing the differences among the simulated climate periods.

We are confident with the fair agreement of the 20-km GCM data with the observations/analyses exhibited in Figs. 4 and 5, in spite of the general
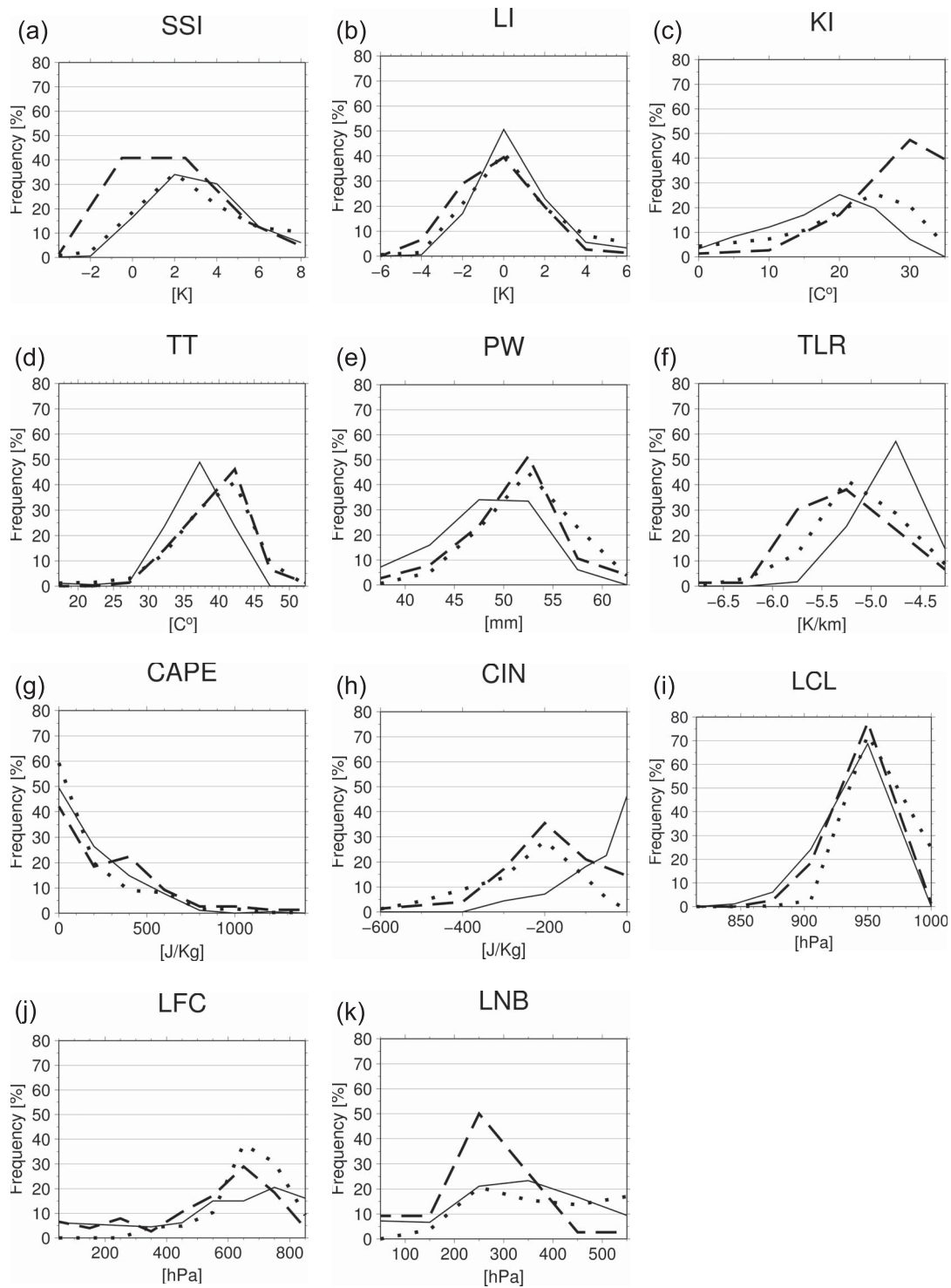
Fig. 5.   The frequency distribution of the stability parameters examined in this study under the synoptically undisturbed condition, obtained from the GCM present simulation (solid lines), the Tateno radiosonde observations (dotted lines), and the MSM analyses (dashed lines).

thinking that the GCM simulations at the resolution of the order of 10 km have inevitably deficiencies in exactly reproducing convective-scale processes and the GCM simulations, even for the present climate, are not able to exactly mimic the real climates. One reason for this favorable agreement is that we are focusing on the conditions that are the environments for convective-scale processes. Therefore, it is demonstrated that the GCM outputs are useful in investigating the environmental characteristics under the synoptically undisturbed conditions. We will further examine the characteristics of environmental stability and precipitation in the GCM present climate in the following.

3.2 Characteristics of precipitation and environmental stability in the present-climate simulation

One-hundred eighty two days that are extracted as the synoptically undisturbed condition will be divided into two categories, that is, no-rain and rain days, depending on rainfalls in the afternoon (i.e., from 1200 to 0000 JST). For dividing these categories, hourly precipitation outputs between 1300 and 0000 JST are used. In NT11, the rain days were defined as having a precipitation intensity of equal to or greater than 1 mm h^{-1} at any grid points within the analysis area during the afternoon hours. However, it was indicated by Kanada et al. (2010b) that the amount of precipitation in the GCM outputs is in general underestimated against the observed rainfalls. In addition, it is reasonable to think that the GCM simulations cannot reproduce quantitatively the convective precipitation with an intensity of a few mm h^{-1} at an hourly timescale owing to a coarse resolution for resolving such convective-scales. Therefore, the direct application of the definition of NT11 to the GCM data may not be appropriate. In order to distinguish no-rain and rain days among the extracted 182 cases from the GCM outputs, the precipitation characteristics from the GCM outputs are examined first.

Figure 6 shows the frequency distributions of the maximum hourly precipitation and the total amount of precipitation during the afternoon hours on the undisturbed days extracted from the GCM present simulation, the AMeDAS observations, and the MSM 3-hour forecasts. A sharp decrease in the frequency with the increase in the precipitation is overall reproduced in the GCM outputs for both the maximum hourly precipitation and the
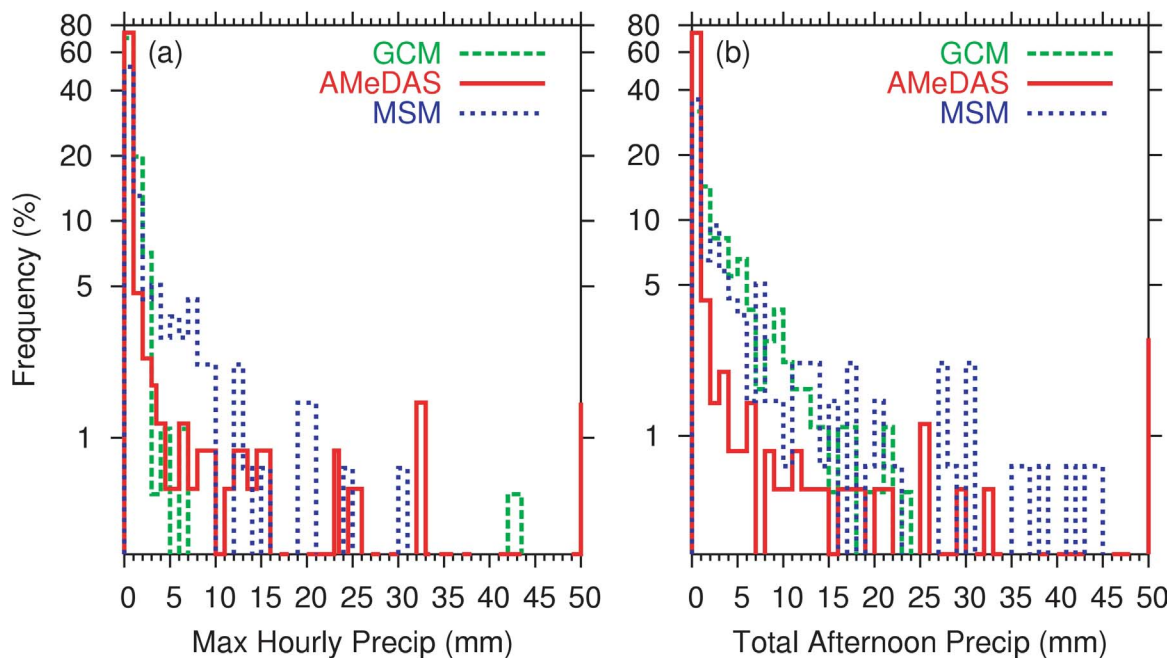

Fig. 6. Frequency distributions of (a) the maximum hourly precipitation during the afternoon and (b) the accumulated precipitation in the afternoon for the undisturbed condition from the GCM present simulation (green), the AMeDAS observations (red), and the MSM forecasts (blue).

total afternoon precipitation. However, the GCM simulation poorly represents the hourly precipitation of greater than about 5 mm h^{-1} (Fig. 6a).

On the other hand, the distribution of total precipitation amounts up to about 25 mm in the AMeDAS and MSM data seems to be better represented in the GCM simulation (Fig. 6b) than the distribution of the maximum hourly precipitation. It is surprising that the frequency distribution of the GCM total precipitation closely captures that of the MSM precipitation. However, it is found that the GCM simulation fails to represent cases with a larger amount of precipitation of greater than 25 mm. In addition, the GCM reproduces more frequencies in representing total precipitation of smaller than 15 mm than do the AMeDAS observations. As shown in Kanada et al. (2010b) in their studies on precipitation characteristics during warm season (from June to October), the GCM present-climate simulation significantly underestimates the frequency of stronger rain events (i.e., greater than 26 mm day^{-1}), while it reproduces weaker rain events relatively well. Because this study focuses on precipitation events in the undisturbed environments, it is expected that the daily precipitation amounts are not so extreme; namely, the total afternoon precipitation for the extracted days is shown to be mostly below 25 mm (Fig. 6b). By our definition the total precipitation during the morning hours is less than 1 mm, and therefore the daily precipitation in the extracted cases is generally less than 25 mm. In this way, the result indicated in Fig. 6b is consistent with the findings of Kanada et al. (2010b).

Consequently, there are both agreements and disagreements in precipitation amounts between the GCM simulation and the observations/analyses. Although there is inevitably a deficiency of the GCM simulation in explicitly resolving convective-scale precipitation, the ability of the GCM in representing the synoptically undisturbed conditions (see Figs. 4 and 5) indicates that the agreement of the total afternoon precipitation between the GCM outputs and the observed climate is evaluated to be fair and is considered to be sufficient for the present analyses on the environmental conditions. These considerations lead us to employ the total afternoon precipitation as a measure to distinguish no-rain and rain cases among the synoptically undisturbed days extracted from the GCM outputs. It should be noted that the precipitation outputs of the present GCM have been used for hydrologic

applications and favorable results have been obtained (e.g., Kim et al. 2010).

In order to distinguish no-rain and rain cases, a certain threshold is used here. The present purpose is to clearly separate the environmental conditions for no-rain and rain events and to evaluate the differences in the mean atmospheric states from the selected cases. Therefore, we apply clearly differentiating thresholds that will at the same time allow sufficient numbers of cases for statistical analyses. No-rain days (denoted as N days) are defined as having the total afternoon precipitation of less than 1 mm at every grid point within the analysis area. On the other hand, rain days (denoted as R days) are defined as having the total precipitation of greater than or equal to 5 mm at any grid points over the analysis area. This setting of the thresholds classifies 84 cases as the N days and 58 cases as the R days, indicating that the both categories include sufficient numbers of cases. This rain categorization is used to identify the differences in the environmental conditions between the N and R days not only in the present but also in the near-future and the future climates represented in the GCM simulations.

To confirm that there are no significant synoptic-scale disturbances on the N and R days, we examine large-scale pressure patterns averaged for each category. The spatial distributions of geopotential height at the 500-hPa level at 0900 JST averaged for the N and R days are shown in Fig. 7 obtained from the MSM analyses and in Fig. 8 obtained from the GCM present-climate simulation. The MSM composites in Fig. 7 clearly demonstrate that the most part of Japan including the Kanto Plain is covered by a high pressure system centered on the Pacific just south of the Japanese Islands on both the N and R days. This pressure pattern indicated by the MSM analyses as the real climate is favorably represented in the GCM simulation (Fig. 8). It is also confirmed in Fig. 8 that no significant synoptic-scale low-pressure system appears in the GCM composites for both the N and R days. In addition, the overall agreement shown in Figs. 7 and 8 further supports that the GCM data under the synoptically undisturbed condition capture the environmental characteristics that are seen in the existing climate.

The difference in the environmental characteristics between the N and R days from the GCM outputs is examined here. Figure 9 indicates the environmental atmospheric states at 0900 JST for the
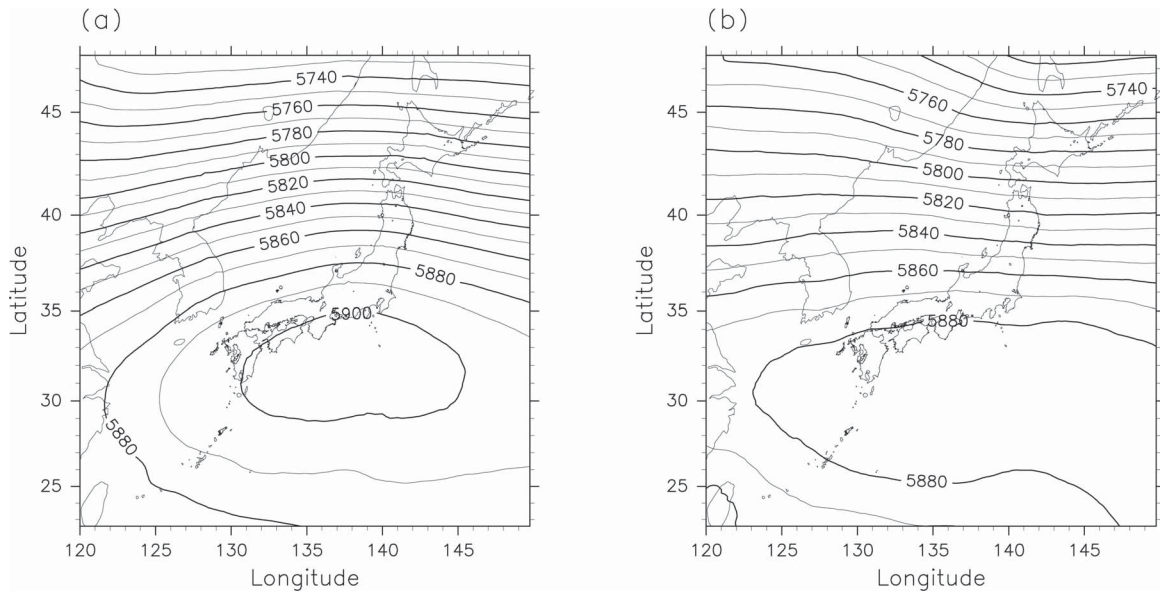
Fig. 7. Geopotential height at the 500-hPa level at 0900 JST averaged for (a) the N days and (b) the R days from the MSM analyses. The contour interval is 10 m.
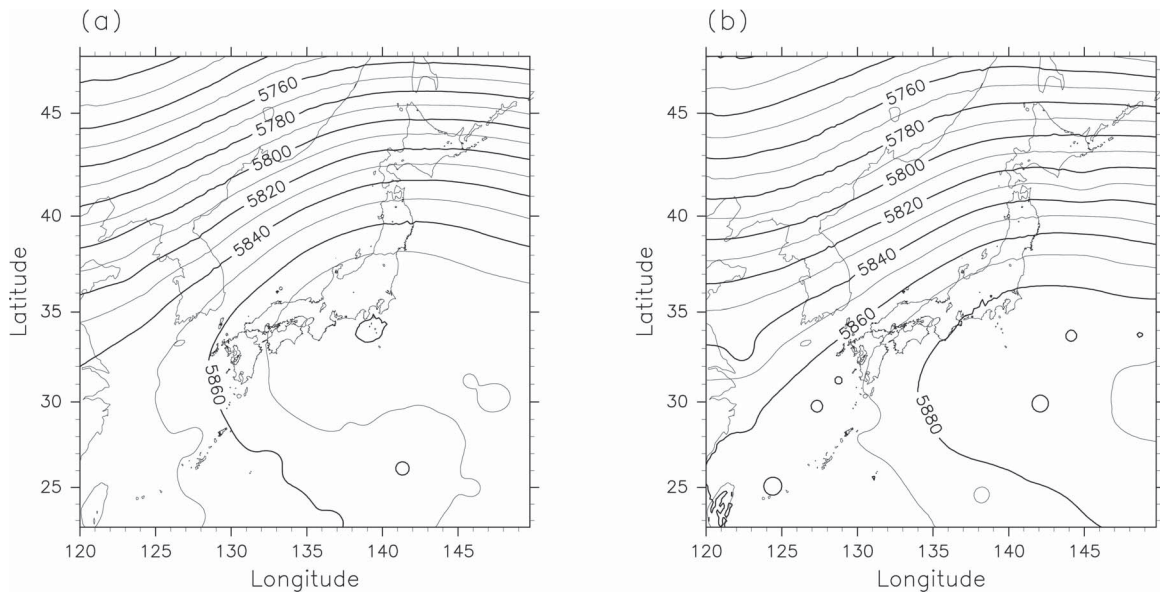

Fig. 8. The same as Fig. 7, except from the GCM present-climate simulation.

N and R days in terms of the vertical profiles of temperature, relative humidity, and water vapor mixing ratio averaged for the chosen days from the present-climate simulation. In the R cases, temperature increases in the lower layer, and both moisture variables, not only mixing ratio but also relative humidity, increase at most of the vertical levels. As will be shown later in this subsection, TLR and PW are more increased on the R days than on the N days. This point is consistently represented in the vertical profiles demonstrated in Fig. 9.

In order to statistically confirm the difference between the R and N days, we use t-test statistic to
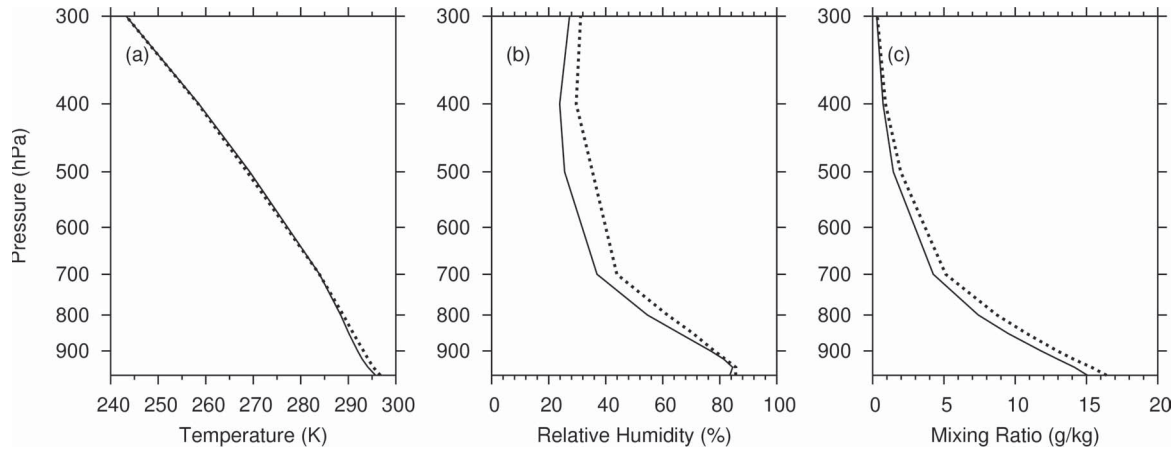
Fig. 9. The vertical profiles of (a) temperature, (b) relative humidity, and (c) water vapor mixing ratio at
0900 JST averaged for the N (thin solid line) and the R (dotted line) days under the synoptically un-
disturbed condition in the present climate of the GCM simulation.

verify the statistical significance, as was done in NT11. Test statistic, T, is defined as:

$$T = |x_A - x_B| \cdot \left(\frac{\sigma_A^2}{n_A} + \frac{\sigma_B^2}{n_B} \right)^{-1/2}, \qquad (1)$$

where x_A and x_B are the means for category A and B, respectively, σ_A and σ_B the standard deviations, n_A and n_B denote the number of cases in each category. When T is larger than a certain threshold, a significant difference between the categories is statistically indicated. A larger value of T means that the difference between each category is more significant. In this study, a significance level is evaluated at the 5-% level.

Figures 10a and 10b show the vertical distribution of the differences of temperature and relative humidity at 0900 JST between the N and R days represented in the present-climate simulation. The temperature in the lower layer (in the middle layer) is higher (lower) in the R days than in the N days. On the other hand, the relative humidity throughout the deep troposphere is higher in the R days than in the N days; the largest difference is seen at around the 500-hPa level. The characteristics of these differences are quite similar to those found by NT11 from the MSM analyses and the radiosonde observations.

The statistical significances of these differences are evaluated at each level. In Figs. 10c and 10d, we examine the vertical profile of the T values for the differences shown in Figs. 10a and 10b. For the temperature differences, the T values exceeding the

significance level are found below the 800-hPa level and at the 500-hPa level. This indicates that the low-level higher temperature and the middle-level lower temperature in the R days than in the N days are statistically significant. For the relative humidity difference, the T values exceed the significance level in the middle layer, with the maximum found at the 500-hPa level. Thus, the humidity at the middle levels is statistically higher in the R days than in the N days. Although the vertical distributions of the statistical significance are a little different from those obtained from the MSM analyses by NT11, the middle-level and low-level significance for the temperature difference and the middle-level significance for the relative humidity difference, which are identified by the MSM analyses, are favorably reproduced in the GCM present-climate simulation.

The results given in this subsection as well as in Section 3.1 strongly indicate that the GCM present-climate simulation well reproduces the characteristics of the environmental stability and its difference between the N and R days under the synoptically undisturbed condition in summer. Furthermore, it is indicated that the evaluation of the environmental characteristics at regional-scales is quite reasonable even with the GCM outputs. Based on the analyses on the GCM present-climate simulation, therefore, we will provide future projections of the changes in the environmental conditions under the synoptically undisturbed conditions in the next subsection.
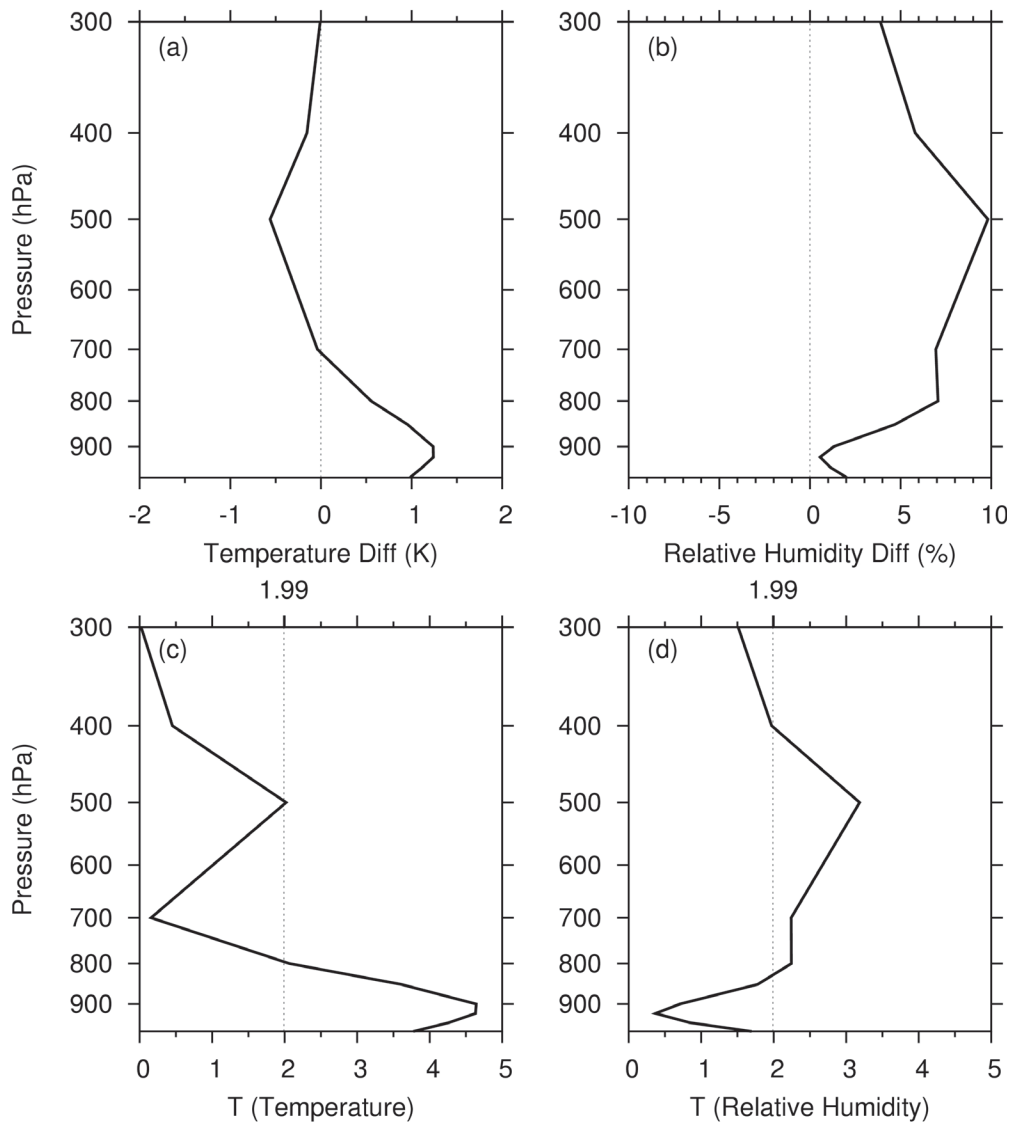
Fig. 10.   The vertical profiles of the mean difference of (a) temperature and (b) relative humidity at 0900 JST
between the categories of the N and the R days, and the T values for (c) the temperature difference and (d)
the relative humidity difference between the two categories, obtained from the GCM present simulation. In
(a) and (b), the positive difference means that the R-day case is larger than the N-day case. In (c) and (d),
the threshold for the statistical significance ($T = 1.99$) is indicated by dotted lines.

3.3   Future projections of environmental stability

The criteria given in Section 2.2 are applied to
the GCM simulation outputs for the present, the
near-future, and the future climates in order to ex-
tract the synoptically undisturbed conditions in
each climate period. In addition, the extracted days
are divided into the N and R days by the rain cate-
gorization defined in Section 3.2. Table 1 summa-
rizes the numbers of the synoptically undisturbed

days and the N and R days in each simulated
period. It is seen that the total number of days ex-
tracted as satisfying a synoptically undisturbed
condition as well as the number of the N days de-
creases from the present to the future climate.

The characteristics of the frequency of precipita-
tion, that is, the hourly maximum and the total
amount during the afternoon hours, under the syn-
optically undisturbed conditions in the present, the

Table 1.   The numbers of the synoptically undisturbed days, the no-rain (N) days, and the rain (R) days in the present, the near-future, and the future climates represented in GCM.

	Present	Near future	Future
Total	182	160	128
N days	84	57	45
R days	58	54	51

near-future, and the future climates are compared in Fig. 11. For both hourly maxima and total amounts of afternoon precipitation, it is difficult to find any pronounced differences among the simulated periods in the frequency distribution. Some differences are seen for the total amount of afternoon precipitation; the number of cases with the total amount of greater than 5 mm appears to slightly increase with the future period. However, the tendency with time is not clearly identified.

As mentioned in Section 3.2 in relation to Fig. 6, it is reasonable to assume that the weaker rain events (with the amount of less than 26 mm day^{-1})

are represented in the GCM simulations relatively well. Figure 11b confirms that almost all the extracted days have total precipitation of below 25 mm day^{-1}. In addition, the environmental conditions should be better represented than quantitative precipitation amounts, considering that the downscaling experiments with a nonhydrostatic RCM nested in the present GCM using a nudging method (which means that the background states in RCM are essentially the same as in GCM) are successful in quantitatively representing rainfall (Kanada et al. 2008, 2010b). Therefore, the environmental atmospheric conditions at regional-scales are appropriately evaluated with the GCM climate simulations. In the followings, we focus on the changes of the environmental stability in future climates.

The mean vertical profiles of temperature, relative humidity, and water vapor mixing ratio under the synoptically undisturbed conditions in the simulated present, near-future, and future climates are exhibited in Fig. 12. Temperature and mixing ratio at all the levels increase with the future period. On the other hand, relative humidity, especially below the 600-hPa level, does not largely vary among the simulated period.
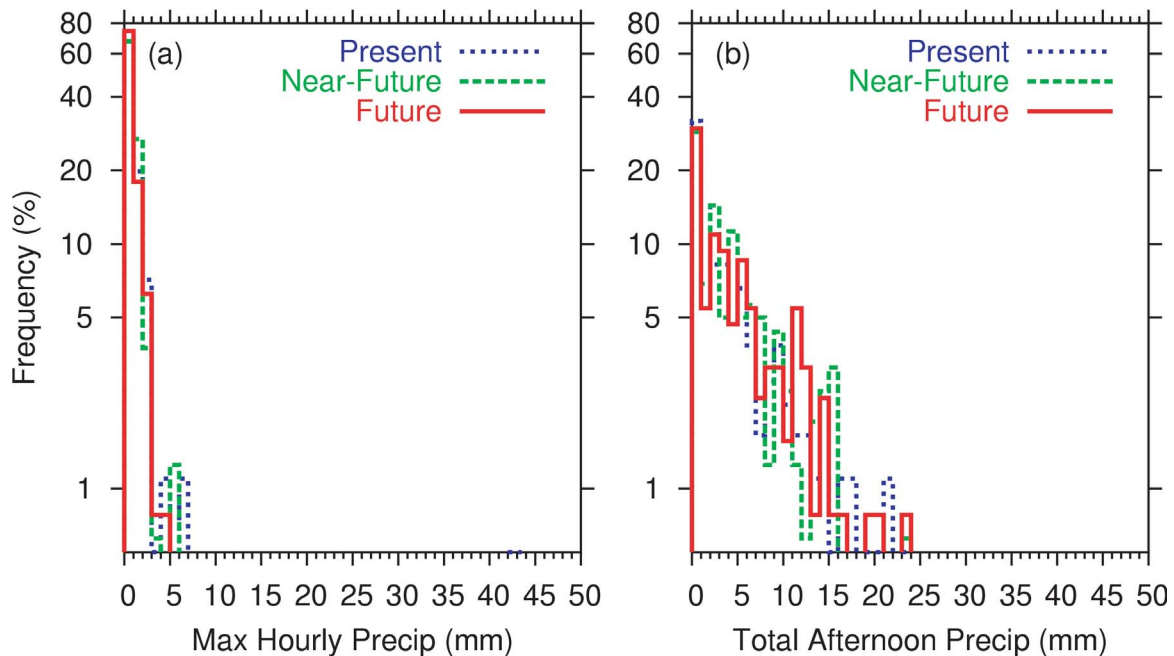

Fig. 11.   The frequency distributions of (a) the maximum hourly precipitation during the afternoon and (b) the accumulated precipitation in the afternoon for the undisturbed condition from the present (blue), the near-future (green), and the future (red) climate simulations of the GCM.
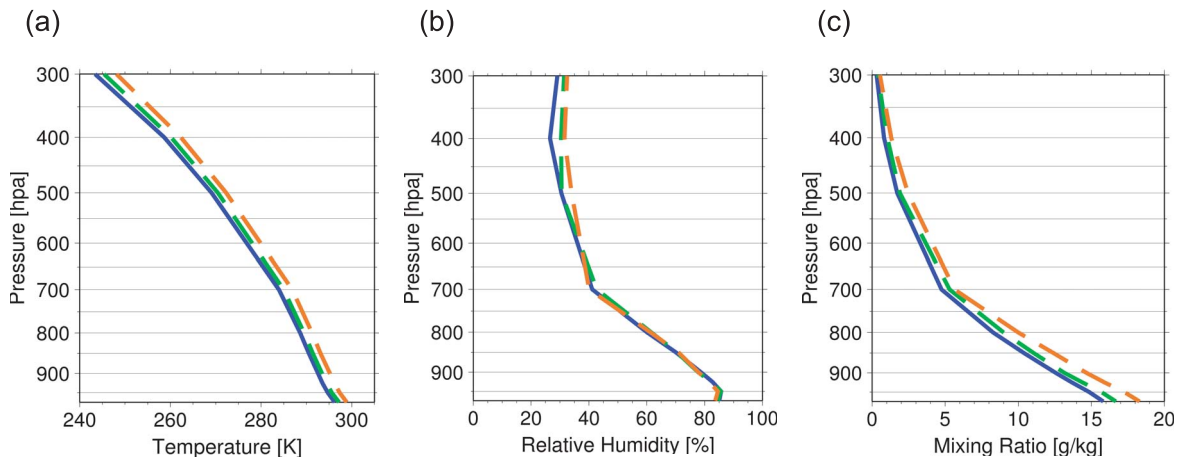
(a)

(b)

(c)

Fig. 12.   The vertical profiles of (a) temperature, (b) relative humidity, and (c) water vapor mixing ratio at 0900 JST averaged for the synoptically undisturbed condition in the present (blue), the near-future (green), and the future (red) climate simulations.

Figure 13 demonstrates the vertical profiles of the differences of temperature, relative humidity, and water vapor mixing ratio averaged for the undisturbed cases over each simulated period, and also the profiles of the T values that indicate the statistical significance for these differences. Although there are differences in the relative humidity (Fig. 13b) between the near-future (the future) and the present climate, the existence of the statistical significance for the differences is not identified (Fig. 13e). On the other hand, the temperature and mixing ratio increase with the future period (Figs. 13a and 13c). The T values for these differences in temperature and mixing ratio shown in Figs. 13d and 13f exceed the significance level, which means that those differences are statistically significant. Considering that the relative humidity change is not significant (Fig. 13e) and is basically none (Fig. 12b), the increase in mixing ratio occurs in response to the increase in temperature under the condition regulated by the Clapeyron-Clausius equation.

The vertical profiles of temperature and moisture for all the August days at 0900 JST in each climate period were also examined. The differences in the August means of the temperature and moisture profiles between the present and the future climates were found to be significantly smaller than those shown in Fig. 13. Therefore, environmental changes in summer are more enhanced under the synoptically undisturbed conditions than under the mean conditions throughout the total August days. Further discussion on this topic is given in Section 4.

The changes in the temperature and moisture profiles will lead to the changes in stability indices and parameters. Temperature lapse rate, total moisture, one of stability indices, and an unstable energy parameter are examined here. Figure 14 shows the frequency distributions of TLR, PW, LI, and CAPE for the periods of the present, the near-future, and the future climate. The temperature lapse rate becomes more stable in the future than in the present climate, while the precipitable water vapor content increases in the future than in the present. LI and CAPE seem to indicate more unstable values with the future period. The changes in TLR and PW seem to be consistent with the changes indicated in Fig. 12.

The statistical significance for the differences in the means of the stability parameters between the present and the near-future (the future) climate is examined by t-test statistic. The T value indicating the significance level for this analysis is 1.96. The parameters that exceed the significance level for the differences between the present and the near-future are TLR ($T = 2.73$), PW ($T = 3.62$), and TT ($T = 1.97$): TLR and TT become smaller with the future period; while PW larger. For the differences between the present and the future, the parameters exceeding the significance level are TLR ($T = 3.53$), PW ($T = 7.11$), CAPE ($T = 4.27$), CIN ($T = 2.73$), LNB ($T = 2.23$), and LI ($T = 2.14$): CAPE, CIN, and PW become larger with the future period; TLR and LI become smaller; and LNB becomes higher. This result indicates that the atmo-
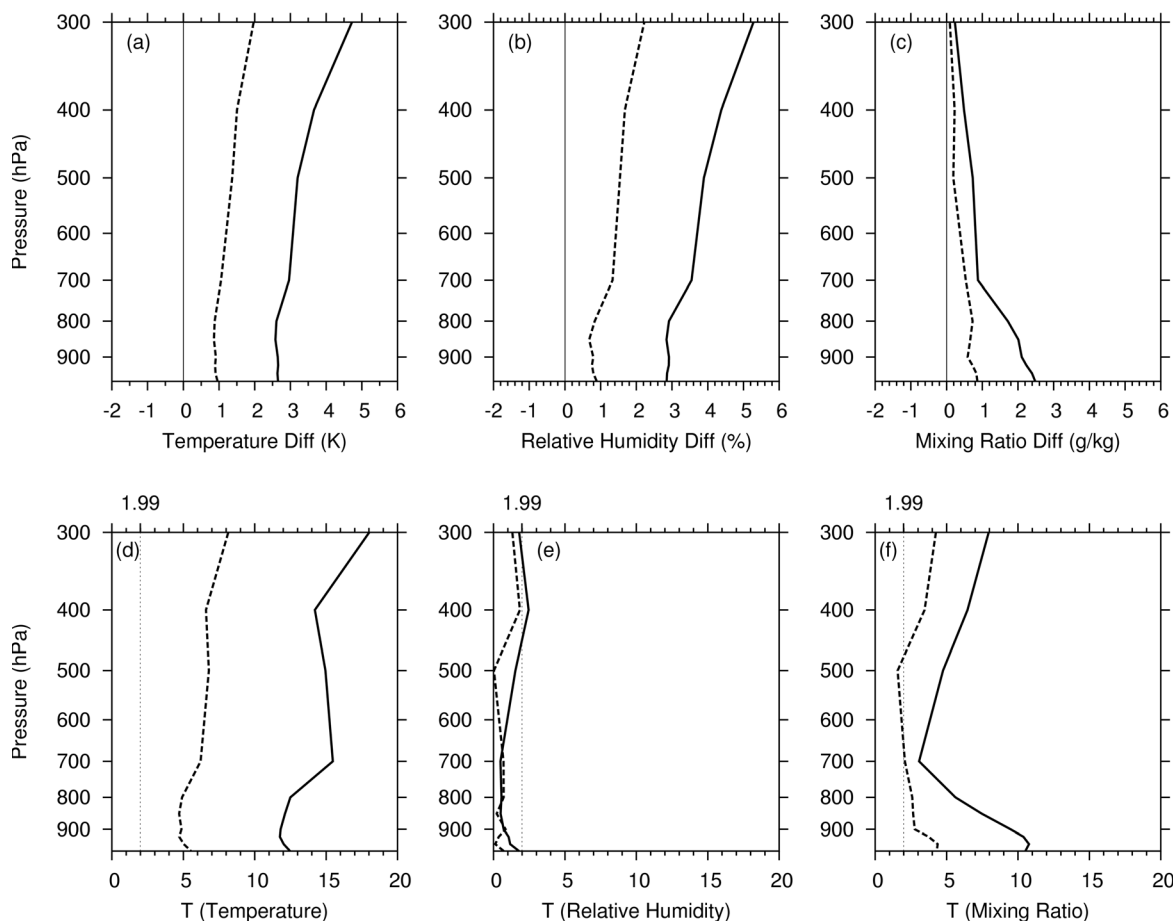
Fig. 13. The vertical profiles of the mean differences of (a) temperature, (b) relative humidity, and (c) water vapor mixing ratio between the present and the near future climate (dashed lines) and between the present and the future climate (solid lines), and the T values for (d) the temperature difference, (e) the relative humidity difference, and (f) the mixing ratio difference obtained from the undisturbed conditions in the GCM simulations. In (a)–(c), the positive difference means that the future (near-future) case is larger than the present case. In (d)–(f), the threshold for the statistical significance ($T = 1.99$) is indicated by dotted lines.

sphere becomes more unstable in terms of CAPE, PW, and LNB with the future while becomes more stable in terms of TLR and CIN. Coupled effects in the lapse rate decrease and the moisture increase result in shifting LI towards more unstable. In this way, this statistical analysis clearly demonstrates that the differences found in the frequency distributions in Fig. 14 are significant in a statistical sense.

Furthermore, the differences of the stability parameters between the N and R days in each simulated climate are examined. Figure 15 compares the frequency distribution of the parameters, having distinct features identified in Fig. 14 and t-test statistics, among the three simulated climate peri-

ods by classifying the N- and R-day cases. Compared with those shown in Fig. 14, the differences in the representation of the stability parameters among the simulated climate periods are more enhanced through distinguishing whether or not total afternoon precipitation satisfies the defined threshold. With the future period, CAPE becomes larger, TLR becomes smaller, and PW becomes larger not only on the N days but also on the R days. The increases in CAPE and PW with time seem to be more distinct in the R days than in the N days. An interesting point is that the magnitude of TLR is found to decrease even in the R days with the simulated period, despite that on rainy days convection
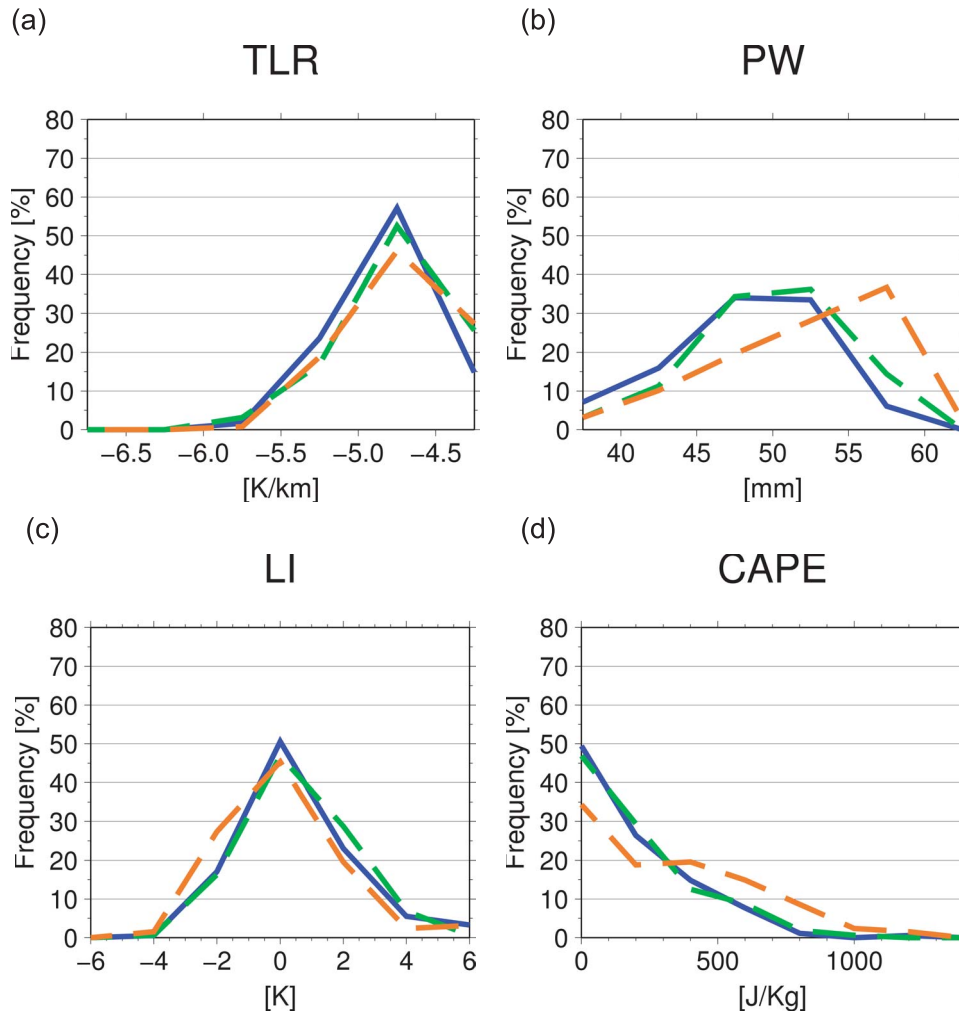
(a)

TLR

(b)

PW

(c)

LI

(d)

CAPE

Fig. 14.   The frequency distribution of (a) TLR, (b) PW, (c) LI, and (d) CAPE for the synoptically un-
disturbed conditions in the present (blue), the near-future (green), and the future (red) climate simulations.

is expected to be more active; however, the value of
TLR unanimously shifts toward unstable on the R
days in each climate period.

   The t-test statistic was carried out for the differ-
ences in the means of the stability parameters be-
tween the N and R days, as was done in NT11.
The T values for the differences in the parameter
means between the rain categories in each simu-
lated period are summarized in Table 2. The pa-
rameters exceeding the significance level for all the
simulated periods are CAPE, LFC, SSI, LI, KI,
TT, TLR, and PW. NT11 showed that these pa-
rameters had statistical significance in distinguish-
ing their mean values on the no-rain and rain days.
The analysis for the present climate indicates that

the results obtained from the GCM outputs are con-
sistent with the results obtained from the analyses
of the radiosonde and MSM data. This also gives
reliability on the analyses for the near-future and
the future climates.

   The analyses of the statistical significance shown
in Table 2 further indicate that the environmental
stability settings in terms of the stability parameters
that distinguish no-rain and rain events are basi-
cally unchanged between the present and the future
climate period. In other words, it is suggested that
the environmental characteristics favorable for af-
ternoon precipitation under the synoptically un-
disturbed conditions will not change under global
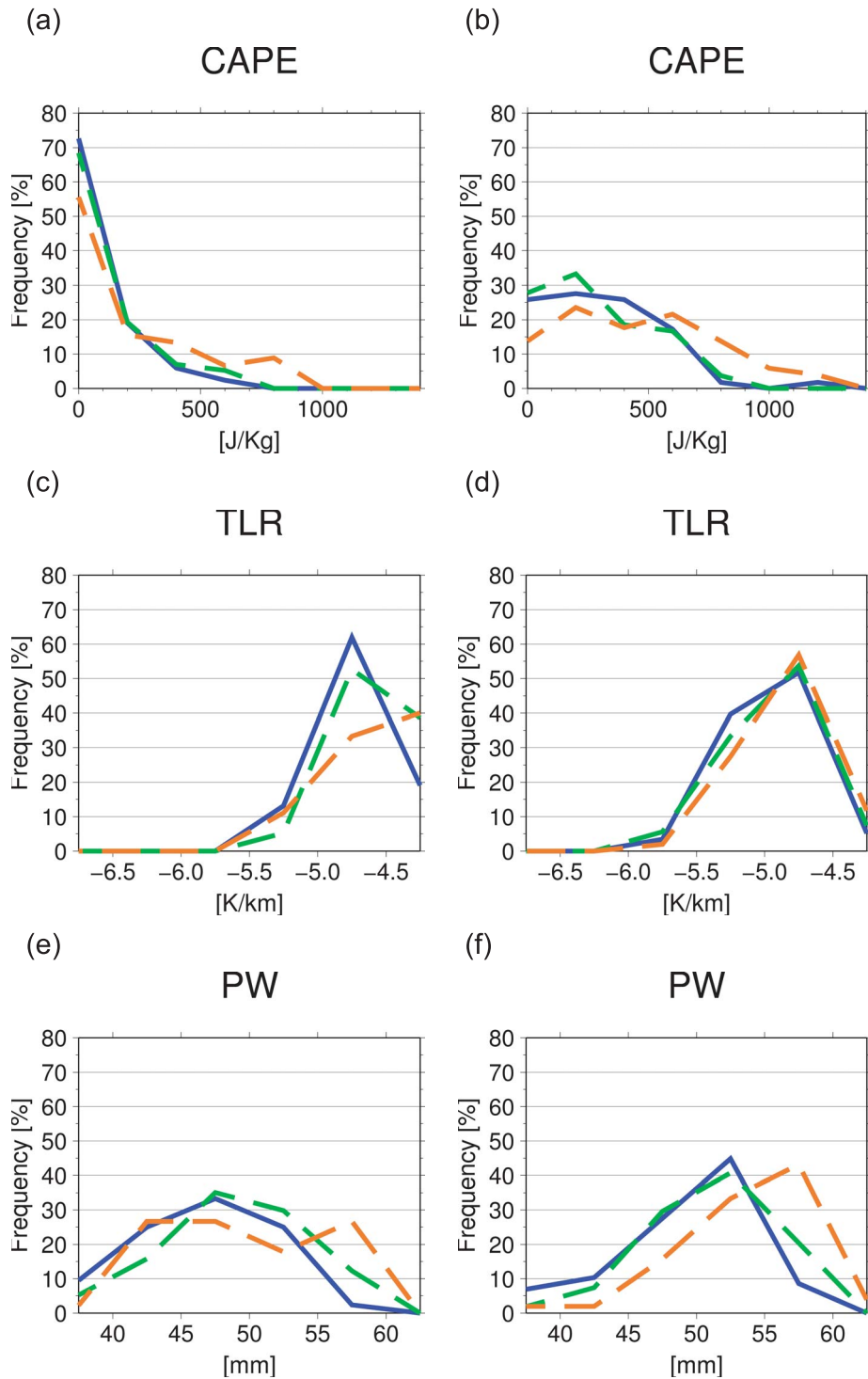warming.

Fig. 15.   The frequency distributions of (a) CAPE, (c) TLR, and (e) PW in the present (blue), the near-future (green), and the future (red) climates for the N days, and those of (b) CAPE, (d) TLR, and (f) PW in the R days.

Table 2. The T values for the differences in the stability parameters between the N and R days in the present, the near-future, and the future climate simulations. The significance level is $T = 1.97$. The bold digits satisfy this significance level.

	CAPE	CIN	LCL	LFC	LNB	SSI	LI	KI	TT	TLR	PW
Present	**6.32**	1.74	0.72	**3.80**	0.27	**4.96**	**6.86**	**3.90**	**5.69**	**5.68**	**3.43**
Near future	**5.26**	0.93	1.03	**3.31**	0.82	**5.57**	**6.26**	**5.04**	**7.12**	**6.73**	**2.08**
Future	**4.51**	1.27	1.15	**5.39**	0.57	**5.92**	**5.22**	**5.50**	**6.91**	**5.66**	**4.04**

4. Discussion

The present analyses on the environmental stability under the synoptically undisturbed conditions from the GCM outputs showed that with the future period the temperature lapse rate in the lower troposphere becomes more stable while precipitable water vapor and CAPE become larger (Fig. 14). The increase in precipitable water vapor was due to the increase in water vapor mixing ratio at all the vertical levels (Fig. 13c), while the decrease in temperature lapse rate was due to the larger increase in temperature at higher levels (Fig. 13a). These changes were found to be statistically significant. As stated in Section 3.3, these environmental changes appear to be more enhanced under the synoptically undisturbed conditions than under the composited August conditions in each climate period.

Figure 16 demonstrates the vertical distributions of the differences of temperature and moisture between the present and the future (near future) cli-

mates for all the August days at 0900 JST. There are slight increases in temperature and water vapor mixing ratio from the present to the future climate: temperature increased by less than 2 K at all the levels; and mixing ratio increased by less than 1.5 g kg^{-1} at the lowest level and by less than 1.0 g kg^{-1} above the 800-hPa level. In addition, the differences between the present and the near-future climate are very small. Although statistical significance test indicated that the differences in temperature and mixing ratio were significant, those differences for the August composites are significantly smaller than the differences for the undisturbed conditions. Furthermore, the temperature differences are almost the same at all the levels between 975 hPa and 500 hPa, which means that TLR is not changed with the future time for all the cases in August. Therefore, the decrease of the temperature lapse rate in the lower troposphere in the future climate seems to be a unique feature for the undisturbed conditions in August.
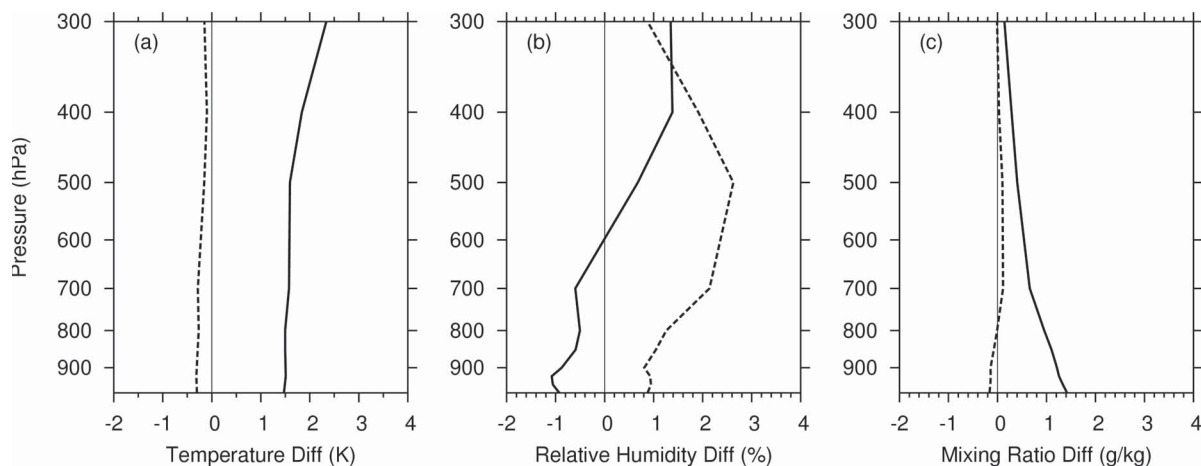

Fig. 16. The vertical profiles of the mean differences of (a) temperature, (b) relative humidity, and (c) water vapor mixing ratio between the present and the near future climates (dashed lines) and between the present and the future climates (solid lines) for all the days in August during each climate period.
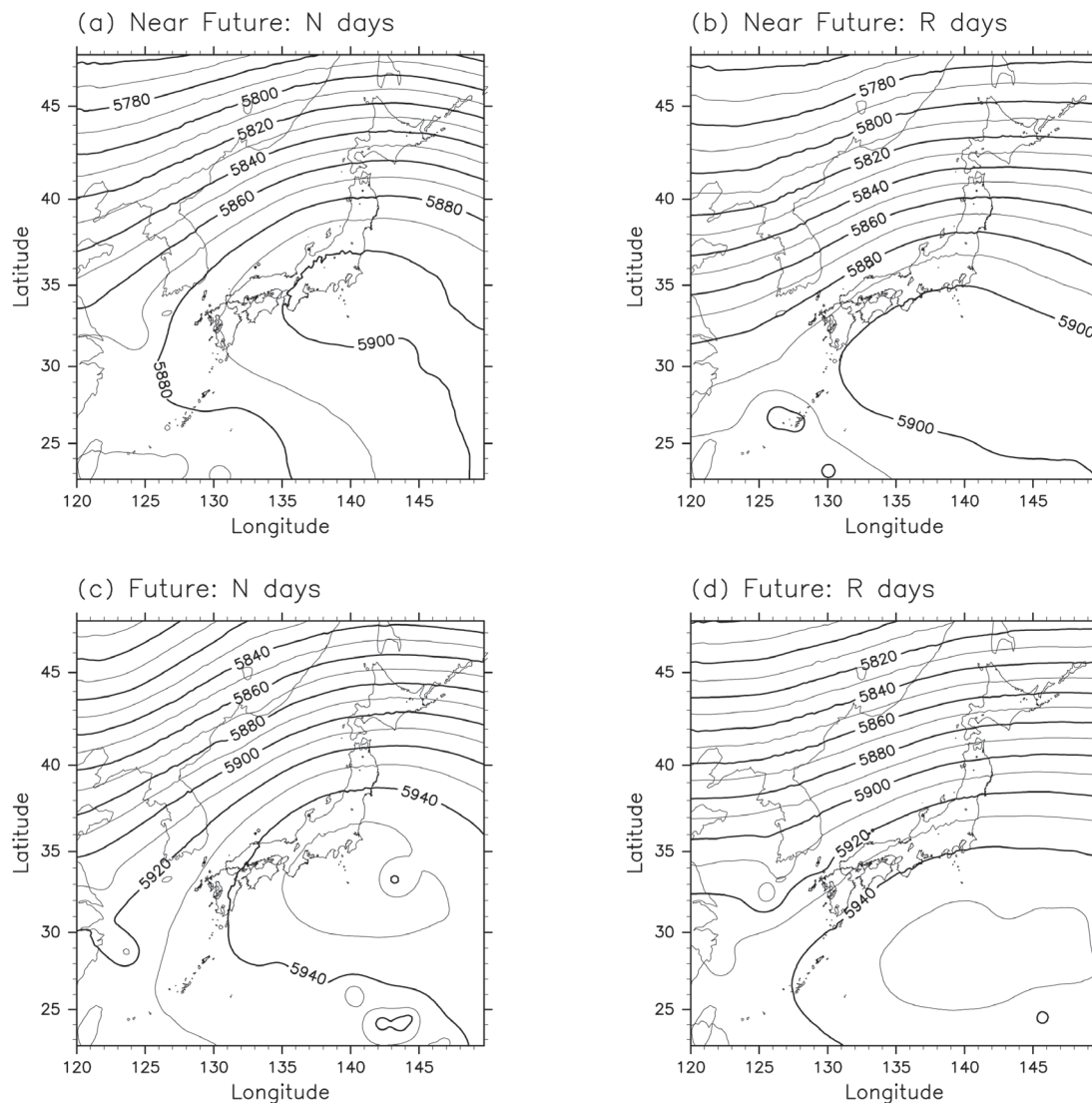
Fig. 17. The same as Fig. 8, except from the near future-climate simulation for (a) the N days and (b) the R days and from the future-climate simulation for (c) the N days and (d) the R days.

As demonstrated in Fig. 8, the undisturbed conditions in August are resulted from the existence of a subtropical high-pressure system over the Pacific. Synoptic-scale geopotential heights for the N and R days during the near-future and future periods are exhibited in Fig. 17. Compared with the field shown in Fig. 8, the spatial patterns appear to be overall similar among the simulated climate periods. The area of interest, the Kanto Plain, is covered with the subtropical high. For the same rain category, the geopotential heights over the Kanto Plain increase with the climate period, which is in-

dicated to be a manifestation of the future changes in meridional circulation rooted in the Tropics. It is clearly seen that the affected region is not limited to the Kanto Plain but also extended to the southern part of the Japanese islands. Therefore, the changes of the environmental conditions in the Kanto Plain region will appear in the same way in the southern part of the Japanese islands. The decrease of the magnitude of TLR in the future periods is considered to be affected both by the warming in the tropical upper troposphere in the warming climate and by subsidence adiabatic warming in the middle to

upper troposphere over the subtropical-high region.

The precipitation characteristics that are implied from the projected changes in the environmental stability are discussed here. Takemi (2007, 2010) investigated the precipitation characteristics within mesoscale convective systems by changing temperature lapse rate and moisture content as well as shear profile in an idealized simulation setup where the base-state atmosphere is horizontally uniform without any external forcing. This idealized setup is regarded as synoptically undisturbed, since only convective forcing is an initial thermal (and the resultant self-organizing effects). The weak shear condition (i.e., 5 m s^{-1} difference only in the lowest 2.5 km) examined in Takemi (2007, 2010) corresponds to the synoptically undisturbed conditions examined in this study. Their results indicated that with the same CAPE environment convection intensity (represented as updraft strength) and mean precipitation decrease as temperature lapse rate decreases, and also indicated that with the similar lapse rate convection intensity and mean precipitation increase as CAPE increases. In the projected environments in the future periods, it was found that temperature lapse rate decreases but CAPE increases. These contrasting effects of the lapse rate decrease and the CAPE increase will be canceled with each other in the future-climate environments. Based on the results of Takemi (2007, 2010), convection intensity and mean precipitation will not decrease. Thus, it is implied that precipitation amount would be maintained or even intensified in the future climates.

An interesting result in Takemi (2010) was that the maximum precipitation intensity increases with the decrease in temperature lapse rate while with CAPE being unchanged. On the other hand, the present analyses of the GCM data indicated that both static stability and CAPE increases. Applying the result of Takemi (2010) to the projected changes in the environmental stability, the precipitation intensity in short time-scales is suggested to increase. This point should be quantitatively evaluated from the results of non-hydrostatic RCM simulations without cumulus parameterizations.

5. Conclusions

This study investigated the characteristics of the environmental stability for afternoon convective precipitation that would develop under synoptically undisturbed conditions in summer with the use of the outputs of GCM climate simulations and evalu-

ate the changes in the stability conditions under warming climates at a regional-scale. The GCM simulations were done by a super-high-resolution atmospheric GCM, MRI-AGCM3.2S, at about 20-km resolution (Kitoh et al. 2009). The climate simulation outputs that were used in this study corresponded to three 25-year periods: 1980–2004 for the present climate; 2020–2044 for the near-future climate; and 2075–2099 for the future climate. The simulations for future climates were done with the IPCC A1B emission scenario that induces global warming. The Kanto Plain was chosen as the area of interest, because there have been a sufficient number of the previous studies that examined the environmental stability over the region and it was useful to evaluate the performance of the GCM outputs against the observations and the analyses. To diagnose the environmental conditions, some of the commonly used stability parameters and indices were used. The future projections of the changes in the environmental stability for the afternoon precipitation events over the region were provided.

The comparison of the GCM present climate extracted as the synoptically undisturbed conditions with the corresponding states revealed by the radiosonde observations at Tateno in the Kanto Plain and the MSM analyses indicated that the GCM present climate well reproduced the characteristics of the temperature and moisture profiles, the stability parameters, and also daily precipitation amounts up to 25 mm. These favorable agreements of the GCM outputs with the real, existing climates enabled us to investigate and evaluate the changes in the environmental stability under global warming.

In the future climates, temperature lapse rate decreased in the lower troposphere, while water vapor mixing ratio increased throughout the deep troposphere. The changes in the temperature and moisture profiles resulted in the increase in both precipitable water vapor and CAPE, which were evaluated as statistically significant. These projected changes were indicated to be enhanced with the future period.

Furthermore, the differences of the stability parameters between the no-rain and the rain days under the synoptically undisturbed condition in each simulated climate period were examined. The statistical analyses for these differences indicated that the environmental conditions in terms of the stability parameters that distinguish no-rain and rain events are basically unchanged between the

present and the future (including the near-future) climate. This result suggests that the environmental characteristics favorable for afternoon precipitation in the synoptically undisturbed environments will not change under global warming. The present results further suggest that the potential for thunderstorm activity is not significantly affected in the future climates despite the increase of moisture content; this is considered to be due to the contrasting effects of the moisture increase and the lapse rate decrease.

The present study focuses on the characteristics and future changes of the environmental stability for convective precipitation, but not on the precipitation amount itself. Precipitation characteristics in future climates under global warming have been actively investigated by non-hydrostatic regional climate models such as in Kanada et al. (2008, 2010b). Combining those RCM results with the present analyses will give more in-depth understanding on the behavior of precipitation under global warming.

Acknowledgments

References

Bengston, L., and K. I. Hodges, 2011: On the evaluation of temperature trends in the tropical troposphere. *Clim. Dyn.*, **36**, 419–430.

Bluestein, H. B., 1993: *Synoptic-Dynamic Meteorology in Midlatitudes, Vol. II*, Oxford Univ. Press, 594 pp.

Bluestein, H. B., and M. H. Jain, 1985: Formation of mesoscale lines of precipitation: Severe squall lines in Oklahoma during the Spring. *J. Atmos. Sci.*, **42**, 1711–1732.

Christy, J. R., W. B. Norris, R. W. Spencer, and J. J. Hnilo, 2007: Tropospheric temperature change since 1979 from tropical radiosonde and satellite measurements. *J. Geophys. Res.*, **112**, D06102, doi:10.1029/2005JD006881.

Chuda, T., and H. Niino, 2005: Climatology of environmental parameters for mesoscale convections in Japan. *J. Meteor. Soc. Japan*, **83**, 391–408.

Del Genio, A. D., M.-S. Yao, and J. Jonas, 2007: Will moist convection be stronger in a warmer climate? *Geophys. Res. Lett.*, **34**, L16703, doi:10.1029/ 2007GL030525.

Fu, Q., S. Manabe, and C. M. Johanson, 2011: On the warming in the tropical upper troposphere: Models versus observations. *Geophys. Res. Lett.*, **38**, L15704, doi:10.1029/2011GL048101.

Fujibe, F., 1998: Spatial anomalies and long-term changes of precipitation in Tokyo. *Tenki*, **45**, 7–18 (in Japanese).

Fujibe, F., N. Yamazaki, M. Katsuyama, and K. Kobayashi, 2005: The increasing trend of intense precipitation in Japan based on four-hourly data for a hundred years. *SOLA*, **1**, 41–44.

Fujibe, F., N. Yamazaki, M. Katsuyama, and K. Kobayashi, 2006: Long-term changes in the diurnal precipitation cycles in Japan for 106 years (1898–2003). *J. Meteor. Soc. Japan*, **84**, 311–317.

Fujibe, F., H. Togawa, and M. Sakata, 2009: Long-term change and spatial anomaly of warm season afternoon precipitation in Tokyo. *SOLA*, **5**, 17–20.

IPCC, 2007: *Climate Change 2007: The Physical Science Basis*. Cambridge University Press, Cambridge, United Kingdom, 996 pp.

Iwasaki, H., 2010: Recent positive trend in heavy rainfall in eastern Japan and its relation with variations in atmospheric moisture. *Int. J. Climatol.*, doi: 10.1002/joc.2269.

Iwashima, T., and R. Yamamoto, 1993: A statistical analysis of the extreme events: long-term trend of heavy daily precipitation. *J. Meteor. Soc. Japan*, **71**, 637–640.

Kamiguchi, K., A. Kitoh, T. Uchiyama, R. Mizuta, and A. Noda, 2006: Changes in precipitation-based extremes indices due to global warming projected by a global 20-km-mesh atmospheric model. *SOLA*, **2**, 64–67.

Kamiguchi, K., O. Arakawa, A. Kitoh, A. Yatagai, A. Hamada, and N. Yasutomi, 2010: Development of APHRO_JP, the first Japanese high-resolution daily precipitation product for more than 100 years. *Hydro. Res. Lett.*, **4**, 60–64.

Kanada, S., C. Muroi, Y. Wakazuki, K. Yasunaga, A. Hashimoto, T. Kato, K. Kurihara, M. Yoshizaki,

and A. Noda, 2005: Structure of mesoscale convective systems during the late Baiu season in the global warming climate simulated by a non-hydrostatic regional model. *SOLA*, **1**, 117–120.

Kanada, S., M. Nakano, S. Hayashi, T. Kato, M. Nakamura, K. Kurihara, and A. Kitoh, 2008: Reproducibility of maximum daily precipitation amount over Japan using a high-resolution non-hydrostatic model. *SOLA*, **4**, 105–108.

Kanada, S., M. Nakano, and T. Kato, 2010a: Changes in mean atmospheric structures around Japan during July due to global warming in regional climate experiments using a cloud-system resolving model. *Hydro. Res. Lett.*, **4**, 11–14.

Kanada, S., M. Nakano, and T. Kato, 2010b: Climatological characteristics of daily precipitation over Japan in the Kakushin regional climate experiments using a non-hydrostatic 5-km-mesh model: Comparison with an outer global 20-km-mesh atmospheric climate model. *SOLA*, **6**, 117–120.

Kanae, S., T. Oki, and A. Kashida, 2004: Changes in hourly heavy precipitation at Tokyo from 1890 to 1999. *J. Meteor. Soc. Japan*, **82**, 241–247.

Kawano, K., Y. Hirokawa, and H. Ohno, 2004: Diagnosis of airmass thunderstorm days using radiosonde data: The summer Kanto area under the Pacific subtropical anticyclone. *Tenki*, **51**, 17–30 (in Japanese).

Kim, S., Y. Tachikawa, E. Nakakita, and K. Takara, 2010: Hydrologic evaluation on the AGCM20 output using observed river discharge data. *Hydro. Res. Lett.*, **4**, 35–39.

Kimoto, M., N. Yasutomi, C. Yokoyama, and S. Emori, 2005: Projected changes in precipitation characteristics around Japan under the global warming. *SOLA*, **1**, 85–88.

Kitoh, A., and T. Uchiyama, 2006: Changes in onset and withdrawl of the east Asian summer rainy season by multi-model global warming experiments. *J. Meteor. Soc. Japan*, **84**, 247–258.

Kitoh, A., T. Ose, K. Kurihara, S. Kusunoki, M. Sugi, and KAKUSHIN Team-3 Modeling Group, 2009: Projection of changes in future weather extremes using super-high-resolution global and regional atmospheric models in the KAKUSHIN program: Results of preliminary experiments. *Hydro. Res. Lett.*, **3**, 49–53.

Kusunoki, S., J. Yoshimura, H. Yoshimura, A. Noda, K. Oouchi, and R. Mizuta, 2006: Change of Baiu rain band in Global warming projection by an atmospheric general circulation model with 20-km grid size. *J. Meteor. Soc. Japan*, **84**, 581–611.

Mizuta, R., K. Oouchi, H. Yoshimura, A. Noda, K. Katayama, S. Yukimoto, M. Hosaka, S. Kusunoki, H. Kawai, and M. Nakagawa, 2006: 20-km-mesh global climate simulations using JMA-GSM Model—Mean climate states—. *J. Meteor. Soc. Japan*, **84**, 165–185.

Murakami, H., and B. Wang, 2010: Future change of north Atlantic tropical cyclone tracks: Projection by a 20-km-mesh global atmospheric model. *J. Climate*, **23**, 2699–2721.

Murakami, H., B. Wang, and A. Kitoh, 2011: Future change of western North Pacific typhoons: Projections by a 20-km-mesh global atmospheric model. *J. Climate*, **24**, 1154–1169.

Ninomiya, K., 2009: Characteristics of precipitation in the Meiyu-Baiu season in the CMIP3 20th century climate simulations. *J. Meteor. Soc. Japan*, **87**, 829–843.

Nomura, S., and T. Takemi, 2011: Environmental stability for afternoon rain events in the Kanto plain in summer. *SOLA*, **7**, 9–12.

Santer, B. D., T. M. L. Wigley, C. Mears, F. J. Wentz, S. A. Klein, D. J. Seidel, K. E. Taylor, P. W. Thorne, M. F. Wehner, P. J. Gleckler, J. S. Boyle, W. D. Collins, K. W. Dixon, C. Doutriaux, M. Free, Q. Fu, J. E. Hansen, G. S. Jones, R. Ruedy, T. R. Karl, J. R. Lanzante, G. A. Meehl, V. Ramaswamy, G. Russell, and G. A. Schmidt, 2005: Amplification of surface temperature trends and variability in the tropical atmosphere. *Science*, **309**, 1551–1556.

Santer, B. D., P. W. Thorne, L. Haimberger, K. E. Taylor, T. M. L. Wigley, J. R. Lanzante, S. Solomon, M. Free, P. J. Gleckler, P. D. Jones, T. R. Karl, S. A. Klein, C. Mears, D. Nychka, G. A. Schmidt, S. C. Sherwood, and F. J. Wentz, 2008: Consistency of modelled and observed temperature trends in the tropical troposphere. *Int. J. Climatol.*, **28**, 1703–1722.

Sato, M., and M. Takahashi, 2000: long-term changes in the properties of summer precipitation in the Tokyo area. *Tenki*, **47**, 643–648 (in Japanese).

Sugi, M., A. Noda, and N. Sato, 2002: Influence of the global warming on tropical cyclone climatology: an experiment with the JMA global model. *J. Meteor. Soc. Japan*, **80**, 249–272.

Taguchi, A., K. Okuyama, and Y. Ogura, 2002: The thunderstorm activity observed by SAFIR and its relation to the atmospheric environment over the Kanto area in the summer. Part II: Thunderstorm prediction by stability indices. *Tenki*, **49**, 649–659 (in Japanese).

Takemi, T., 2010: Dependence of the precipitation intensity in mesoscale convective systems to temperature lapse rate. *Atmos. Res.*, **96**, 273–285.

Takemi, T., 2007: Environmental stability control of the intensity of squall lines under low-level shear conditions. *J. Geophy. Res.*, **112**, D24110, doi:10.1029/2007JD008793.

Thorne, P. W., J. R. Lanzante, T. C. Peterson, D. J.

Seidel, and K. P. Shine, 2010: Tropospheric temperature trends: history of an ongoing controversy. *WIREs Climate Change*, **2**, 66–88.

Wakazuki, Y., M. Yoshizaki, K. Yasunaga, C. Muroi, S. Kanada, A. Hashimoto, T. Kato, K. Kurihara, and A. Noda, 2005: Changes in the characteristic features of disturbances appearing in the Baiu frontal zone over western Japan due to global warming. *SOLA*, **1**, 129–132.

Yasunaga, K., M. Yoshizaki, Y. Wakazuki, C. Muroi, K. Kuruhara, A. Hashimoto, S. Kanada, T. Kato, S. Kusunoki, K. Oouchi, H. Yoshimura, R. Mizuta, and A. Noda, 2006: Changes in the Baiu frontal activity in the future climate simulated by super-high-resolution global and cloud-resolving regional climate models. *J. Meteor. Soc. Japan*, **84**, 199–220.

Yonetani, T., 1982: Increase in number of days with heavy precipitation in Tokyo urban area. *J. Appl. Meteor.*, **21**, 1466–1471.

Yonetani, T., 1975: Characteristics of atmospheric vertical structure on days with thunderstorms in the northern Kanto Plain. *J. Meteor. Soc. Japan*, **53**, 139–148.

Yoshizaki, M., C. Muroi, S. Kanada, Y. Wakazuki, K. Yasunaga, A. Hashimoto, T. Kato, K. Kurihara, A. Noda, and S. Kusunoki, 2005: Changes of Baiu (Mei-yu) frontal activity in the global warming climate simulated by a nonhydrostatic regional model. *SOLA*, **1**, 25–28.